Precision Telescope Control System

PTCS/PN/25:

Thermally-Neutral Traditional Pointing Models and Thermal Corrections to Pointing and Focus

Version: 4
Date: August 17,2007

Author: Kim Constantikes

Filename: ptcspn25.doc

Precision Telescope Control System

GBT Archive: PR036
GBT File: PROJECTS
GBT keywords: PTCS, pointing, thermal

Revision History

Ver.	Changes	Date	Initials
1.0	Original	11/11/03	KTC
2.0	Revised analysis, added data from 11/10 and 11/20 experiments	11/26/03	KTC
3.0	Misc. corrections from reviews: DBS, RMP, JC	11/26/03	KTC
4.0	Corrected typo Equation (17), formatting	8/17/07	KTC

Table of Contents

Abstract

The traditional pointing model of the GBT has had acknowledged systematic errors due to the effects of temperature gradients present in the structure while pointing data were collected. We now have a robust structure temperature monitoring system functioning. These data were combined with pointing and tracking data in order to both construct gravity (traditional) pointing models that represent the GBT without gradients and construct thermal pointing and focus correction predictors. The predictors were single-blind tested against data taken in benign conditions and achieved eight hour standard deviation of focus about 1.6 mm, elevation about 3.2", and azimuth 2.4". Trends in focus, elevation, and azimuth were about –0.22 mm/hour, -0.7"/hour, and –0.15"/hour respectively. There may be evidence of azimuth track unevenness in the elevation residuals.

1 Introduction

Thermal distortions of the GBT are one of the largest contributors to pointing and focus errors. GBT design studies, assuming a linear temperature gradient of 5C across the extreme dimension of the GBT, showed thermal gradient pointing errors of 16" due to primary rotation and translation, or of 11" of alidade distortion[1]. Focusing the GBT has been problematic, with frequent focus checks (as often as once per one-half hour) needed and large excursions from the predicted focus position (up to 20+ mm) evident.

The PTCS project has installed 19 precision structural temperature sensors at a variety of locations including alidade, vertical and horizontal feedarms, and BUS (primary backup structure). These sensors and air temperature as sensed by one of the site weather stations were used, along with astrometric inferences of actual pointing and focus[2] from experiments TPTCSRMP030905, TPTCSRMP030911, TPTCSDSB030923, and TPTCSDSB031002, to develop algorithms that predict pointing and focus perturbations due to thermal effects. This memorandum documents the current algorithms, their performance in training on the datasets above, and a single-blind test on data collected during experiment TPTCSRMP031120.

Note that there are ongoing instrument developments that could supplant the correction strategy described below. For example, plans for precision inclinometry of the elevation bearing housings will directly measure what we infer from temperature distributions on the alidade. Insofar as it is desirable to have a robust system that can detect its own errors to a limited extent, and given the possibility that multiple sensor modalities could yield better estimates, we will proceed to complement temperature inferences with direct measurements where possible.

The details of the methods described below can be (and will be) modified to incorporate new or moved temperature sensors as the need becomes apparent. Increased knowledge of the driving mechanisms and the locations (on the structure) of the largest spatial gradients[3] will result in more refined features[4].

---

[1] Tech Memo 52, "Pointing Accuracy", RSI, January 7,2000.

[2] See http://wiki.gb.nrao.edu/bin/view/PTCS/AntennaCharacterization and http://wiki.gb.nrao.edu/bin/view/PTCS/StructuralTemperaturesAnalysisResults.

[3] Thermal imaging is frequently suggested as a mechanism to get better spatial resolution of the GBT spatial and temporal changes in temperature. This method would be ideal for the primary mirror, where the coating is nearly Lambertian and the entire surface might be imaged from a static camera location on the feed arm. A two-color system in the 8-12 micron band would likely be the best bet, avoiding solar signature

2 Focus Corrections

The effects of temperature and gravity on focus position are assumed to be both superposable, i.e., the effect of any one temperature's change is a linear perturbation of focus, and feedarm tip position is linear in the direction of the gravity vector. The following procedure simultaneously estimates thermal and gravity effects, and thus we claim that the resulting gravity model is "thermally-neutral", i.e., is the focus tracking curve for the idealized GBT where there are no thermal gradients.

2.1 Thermal features and gravity terms

We employ the same gravity focus-tracking model as has been previously applied, i.e.,

$$\Delta F = a_1 + a_2 \sin(\phi) + a_3 \cos(\phi), \qquad (1)$$

where ϕ is the telescope elevation angle. ΔF is then the displacement of the subreflector y_s coordinate from its home position. This model compensates subreflector position primarily for bending of the feedarm.

Thermal features are linear combinations of the existing temperature sensors (see Table 1 and Figure 1) that attempt to capture the macro-effects of substructures within the GBT on the correct focus position of the subreflector, force good generalization (prevent overfitting the data, frequently a problem with functional approximation learning techniques), and to reduce the dimensionality of the feature space to a minimum so as to make best use of a limited data set. All features were selected to be differences of some sort to ensure that the resulting predictor of focus does not have any absolute temperature sensitivity: The working assumption is that the GBT homology is good enough that a thermally "flat" (no thermal gradients) GBT will be in focus regardless of the bulk temperature. Note that no alidade temperatures are included since the alidade could only influence focus via imposition of stresses into the tipping structure, and as we will see this is evidently not the case. Through some intuition, insights[5], and discovery via numerical experiments, the following features have been selected.

2.1.1 Primary-subreflector homology

The difference in material thermal expansion coefficient between the primary mirror (steel) and the subreflector (aluminum) can account for some focus shifts:

$$T_1^{(f)} = T_{SR} - \frac{T_{B1} + T_{B2} + T_{B3} + T_{B4} + T_{B5}}{5}. \qquad (2)$$

---

and thus permitting better accuracy during daytime measurements. A single-color system might also suffice, but again should be in the long wave infrared.

[4] I use the term "feature" in the pattern recognition sense: A function of observed parameters that is somehow natural to the problem (in this case a functional approximation) at hand.

[5] The insight that primary "curling" could be a mechanism was Jim Condon's. See "Quick Astronomical Corrections for GBT Pointing and Focus Tracking", PTCS/PN 10, Section 3.

2.1.2 Primary-feedarm homology

Differences in radiative coupling (sun or sky) and differences in convective heat transfer and vertical air temperature lapses can cause the vertical feed arm temperatures to differ from the primary temperature, hence causing a shift in focus:

$$T_2^{(f)} = \frac{T_{F1} + T_{F2} + T_{F3} + T_{F4} + T_{F5}}{5} - \frac{T_{B1} + T_{B2} + T_{B3} + T_{B4} + T_{B5}}{5}. \quad (3)$$

2.1.3 Horizontal feedarm

Expansion or bending of the horizontal feed arm can cause focus errors. Member expansion is approximated by the difference between the sensor on the horizontal feed arm and the elevation bearing on the same side.

$$T_3^{(f)} = \frac{T_{H2} - T_{E1} + T_{H1} - T_{E2}}{2} \quad (4)$$

2.1.4 BUS differentials

The first BUS (primary backup structure) differential feature tries to capture the "curling" effect by computing a spatial gradient-like feature:

$$T_4^{(f)} = \frac{T_{B1} + T_{B2}}{2} - T_{B5}. \quad (5)$$

The terms T_{B1} and T_{B2} are the right and left vertex (hoop 15, rib $\pm$ 440) BUS tempertures, while T_{B1} is the temperature at the center of the primary (hoop 25, rib 000).

The second BUS term tries to measure the translation of the vertex of the BUS in the z direction, i.e., roughly towards the subreflector.

$$T_5^{(f)} = \frac{T_{B1} + T_{B2}}{2} - \frac{T_{E1} + T_{E2}}{2}. \quad (6)$$

Note that the BUS temperature sensors are located at the intersections of support members from the box structure with the BUS members at the upper level, i.e., closest to the primary panels themselves. Hence this feature attempts to measure the expansion of the support members via the difference between BUS and elevation bearing temperatures.

The third feature is similar but applied to the members closer to the center of the primary:

$$T_6^{(f)} = \frac{T_{B3} + T_{B4} + T_{B5}}{3} - \frac{T_{E1} + T_{E2}}{2}. \quad (7)$$

2.2 Training

The correction to focus is approximated as a linear combination of the temperature and gravity terms.

$$\Delta\tilde{F}\left(\phi, T_i^{(f)}\right) = M^{(f)} \times \begin{bmatrix} T_1^{(f)} \\ \cdot \\ \cdot \\ \cdot \\ T_6^{(f)} \\ 1 \\ \sin(\phi) \\ \cos(\phi) \end{bmatrix} = M^{(f)} \times T^{(f)} \quad (8)$$

Where $F\left(\phi, T_i^{(f)}\right)$ is the focus perturbation as a function of elevation angle ϕ and the temperature features $T_i^{(f)}$. The vector $M^{(f)}$ is the linear map from the feature vector T to F. $M^{(f)}$ is estimated from an experimental dataset as follows:

$$\begin{aligned} \left[\Delta F(t_1) \quad \cdots \quad \Delta F(t_n)\right] &= M \times \left[T(t_1) \quad \cdots \quad T(t_n)\right] \\ \tilde{M}^{(f)} &= \left[\Delta F(t_1) \quad \cdots \quad \Delta F(t_n)\right] \times \left[T(t_1) \quad \cdots \quad T(t_n)\right]^{-1} \end{aligned} \quad (9)$$

Where the T matrix is composed of columns of T as above, with the temperatures and elevation angles at times t_i, the inverse of the T matrix is the Moore-Penrose pseudo-inverse, and the row vector ΔF is the measured focus at times t_i. This yields the least-squared-error solution for the linear map $\tilde{M}^{(f)}$.

The results of this estimation are shown in (versus chronologically ordered scan) and (versus Eastern standard time). Data from four datasets (9/5/03, 9/11/03, 10/02/03, and 11/10/03) and both polarizations were used. Data where the Weather 2 station wind speed was greater than 2.5 m/s were discarded. Data outside of an elevation range of 15° to 85° was excluded since lower elevations incur substantial atmospheric errors, and higher elevations may suffer from azimuth tracking errors. Note that the inclusion of North Celestial Pole tracking experiments[6] were

[6] Richard Prestage came up with this innovation: By tracking the a source very close to the celestial north pole we can capture thermal effects over the diurnal cycle, but avoid any gravity effects since the GBT

essential for good generalization of the fitting process. Also note that the focus data as recorded by Prestage and Balser is the actual focus position rather than the difference between best focus and predicted (by the "default" gravity focus tracking curve), and so large elevation dependent residuals are evident.

Measured focus positions are shown as a black "X" and predicted position shown as a red dot in the first subgraph. The fit is for all four datasets, and the abscissa is scan number within the complete set, chronologically ordered. Note that the predictor removes the majority of the trends in focus, and the residual error has a standard deviation of 3.1 millimeters. The bottom subgraph, labeled "Err Est", is an estimate of the internal 1-sigma uncertainty in the experimental measurement: Actual errors are somewhat larger. Also note that () the data are sparse during daylight hours. This is due to the restriction that the site windspeed be less than 4 meters/sec for all data used in the fit. Evidently the likelihood of low windspeeds is smaller during daylight hours.

The elements of the associated map vector and some interpretation are shown in Table 2. "Significance" is the product of a coefficient and the minimum to maximum span of the associated quantity. This is the maximum contribution (in mm) that the term has in focus adjustment over the conditions in which that the dataset was taken. The resultant gravity terms are quite different from the "default" model terms, indicating that the previous model was substantially corrupted by systematic thermal effects. The ranking (in significance) of the thermal terms contains a surprise: The largest thermal contributions are associated with the horizontal feed arm (HFA). A hypothesis for the physical mechanism is that HFA bends, causing substantial up-down motion of the vertical feed arm (VFA). The next largest contributor (BUS F) is consistent with primary curling. The contribution in SR-Pri suggests that primary-subreflector non-homology due to material thermal expansion coefficient differences is significant. Note that all of the coefficients are of reasonable magnitude, indicating millimeters of focus shift per degree C change in the associated temperature feature.

2.3 Testing

The model in the previous section was subjected to a single-blind test. The model was provided to the Software Development Division to implement in the Antenna Manager (the gravity terms) and in a prototype real-time thermal correction code[7]. An overnight run of focus checks were made and post-processed using the model in Table 2. The striking results are shown in Figure 4 and Figure 5 (note that an EDT offset from UDT was used here, in error). Most importantly, the algorithm predicted the focus to a standard deviation of 1.6 mm, with a mean prediction error of 1.2 mm. The linear trend line fit in Figure 4 has a slope of –0.01 mm per scan, or about –0.22 mm per hour! The standard deviation of residual from the trend line is about 1.5 mm. These data include the sunrise thermal transient which is typically more severe than the sundown transient, and the sky was clear at sunup. At this point some configurations were changed in the experiment (not effecting real-time focus corrections) but data collection continued. Even during the day the focus predictor was adjusting focus to with a few millimeters of the optimal (experimentally measured) focus[8].

This result needs more extensive tests to develop confidence in the model, but there is every reason to believe that we can now correctly predict focus position to a few millimeters during observations from just before sunset to just after sunrise. While I leave it to the astronomer

---

pose is (nearly) constant. The method was combined with some laser rangefinder tests where the advantage was that we didn't need to worry about laser rangefinder pointing models.

[7] See the GB Wiki site for information about the implementation.

[8] See Richard and Dana's notes on Project TPTCSRMP031120

experimentalists to render the definitive opinion[9], the 11/20/03 focus tracking appears to safisfy the W band scientific requirement ($\lambda/2$=1.5mm).

3 Elevation Corrections

A similar approach was used to correct elevation for temperature and gravity effects. Since elevation residuals in the datasets are residuals *after* application of the traditional pointing model, any gravity terms fit in this case are indications that the original pointing model was corrupted by temperature variations during the pointing run.

3.1 Thermal features and gravity terms

We use the GBT standard pointing model as the basis set for the gravity terms where

$$\Delta E = -(IE) - (AW)\sin(\theta) + (AN)\cos(\theta) + (HZCZ)\sin(\phi) + (HZSZ)\cos(\phi) \qquad (10)$$

and the coefficients have the usual physical meanings[10] with θ the azimuth angle and ϕ the elevation angle.

3.1.1 BUS

The BUS contribution to elevation error is due to BUS translation in the y direction or rotation around the x axis (both in Lee King's elevation coordinates[11]). Roughly, x is along the elevation axle, z is local up with the GBT pointed at zenith, and y the right-handed coordinate. The system rotates with the tipping structure. The following feature attempts to capture both translation and rotation.

$$T_1^{(e)} = \frac{T_{B3} + T_{B4} + T_{B5}}{3} - \frac{T_{B1} + T_{B2}}{2} \qquad (11)$$

3.1.2 Horizontal feed arm

Bending of the horizontal feed arm around the x axis with respect to the GBT box structure will cause an elevation shift (and also should correlate with a focus change). The following feature is just the average HFA difference from the average elevation bearing temperature.

---

[9] See Condon, "Quick Astronomical Corrections for GBT Pointing and Focus Tracking" for the details.

[10] See the GBT Pointing page.

[11] See GBT drawing C35102M081.

$$T_2^{(e)} = \frac{T_{H2} - T_{E1} + T_{H1} - T_{E2}}{2} \quad (12)$$

3.1.3 Vertical feed arm

VFA differences in the y direction (front-to-back) will cause bending with an elevation pointing effect. The following feature is the left-right average of the front-back temperature difference at the vertex level of the feed arm:

$$T_3^{(e)} = \frac{T_{F2} + T_{F4}}{2} - \frac{T_{F3} + T_{F5}}{2}. \quad (13)$$

3.1.4 Alidade

Temperature differences in the alidade legs can cause rotation of the el bearing castings (and incidentally, the elevation shaft encoder) around the x axis and thus introduce an elevation pointing error. The following feature is the left-right average of the front-back differences:

$$T_4^{(e)} = \frac{T_{A1} + T_{A2}}{2} - \frac{T_{A3} + T_{A4}}{2}. \quad (14)$$

.

3.2 The correction model

The the linear map $M^{(e)}$ is similar to the focus model, with ϕ and θ as elevation and azimuth, respectively:

$$\Delta E\left(\phi,\theta,T_i^{(e)}\right)=M^{(e)}\times\begin{bmatrix}T_1^{(e)}\\ .\\ .\\ .\\ T_4^{(e)}\\ 1\\ \sin(\phi)\\ \cos(\phi)\\ \sin(\theta)\\ \cos(\theta)\end{bmatrix}=M^{(e)}\times T^{(e)}. \qquad (15)$$

.

A slight complication arises in that both elevation and azimuth pointing terms include the AW and AN terms, and for physical reasons they must be constrained to be the same. If they are estimated independently (in separate elevation and azimuth model fits) they will differ slightly (by about three arc seconds). The models for elevation used for the 11/20/03 experiment did use separate fits, and so will not be included here. Rather, we will defer the discussion of training and testing until after the azimuth model is described.

Note that this doesn't take any of the force away from the single-blind test of predictions using the 11/20/03 data since the thermal models and training data remain the same, but does introduce a complication since the "old" model must be reversed out before the new model is applied.

4 Azimuth corrections

4.1 Thermal features and gravity terms

We use the GBT standard pointing model as the basis set for the gravity terms where

$$\Delta A=(CA)+(NPAE)\sin(\phi)+(IA)\cos(\phi)+(AW)\cos(\theta)\sin(\phi)+(AN)\sin(\theta)\sin(\phi) \qquad (16)$$

and the coefficients have the usual physical meanings[10] with θ the azimuth angle and ϕ the elevation angle. Note that ΔA is azimuth on the sky, i.e., cross-elevation.

4.1.1 Alidade

Left-to-right tilts of the alidade will contribute azimuth error, but in a elevation dependent way:

$$T_1^{(a)}=\sin(\phi)\left[\frac{T_{A1}+T_{A3}}{2}-T_{E1}-\frac{T_{A2}+T_{A4}}{2}+T_{E2}\right]. \qquad (17)$$

.

4.1.2 Horizontal feed arm

Left-to-right bending of the HFA can also introduce azimuth pointing errors:

$$T_2^{(a)} = \frac{T_{H2} - T_{E1} - T_{H1} + T_{E2}}{2}. \quad (18)$$

4.1.3 BUS

BUS contributions to azimuth pointing error are due to translation in the x direction or rotation around the y axis (again, in elevation coordinates). The following feature attempts to capture both via the differential expansions of the BUS support members:

$$T_3^{(a)} = \frac{T_{B1} + T_{B4}}{2} - T_{E1} - \frac{T_{B2} + T_{B3}}{2} + T_{E2}. \quad (19)$$

4.1.4 Vertical feed arm

Finally, the VFA contribution to azimuth error is the front-back average of the left-right difference:

$$T_4^{(a)} = \frac{T_{F2} + T_{F3}}{2} - \frac{T_{F4} + T_{F5}}{2}. \quad (20)$$

4.2 The correction model

The the linear map $M^{(a)}$ is similar to the elevation model, with ϕ and θ as elevation and azimuth, respectively:

$$\Delta A\left(\phi,\theta,T_i^{(a)}\right)=M^{(e)}\times\begin{bmatrix} T_1^{(a)} \\ . \\ . \\ . \\ T_4^{(a)} \\ 1 \\ \sin(\phi) \\ \cos(\phi) \\ \cos(\theta)\sin(\phi) \\ \sin(\theta)\sin(\phi) \end{bmatrix}=M^{(a)}\times T^{(a)}. \qquad (21)$$

5 Train and test of the coupled azimuth and elevation models

Data from four datasets (9/5/03, 9/11/03, 10/02/03, and 11/10/03) and both polarizations and both forward and backwards scans were used to compute the least squares fit of the elevation and azimuth models. Data where the Weather 2 station wind speed was greater than 2.5 m/s were discarded. Data outside of an elevation range of 15° to 85° was excluded since lower elevations incur substantial atmospheric errors, and higher elevations may suffer from azimuth tracking errors. Note that the inclusion of North Celestial Pole tracking experiments were essential for good generalization of the fitting process.

5.1 Elevation results

Figure 6 shows the result of training the elevation model, and Table 3 has the corresponding model coefficients and significances. The residual elevation prediction error in training is 3.4", a factor of 3 reduction from the uncorrected elevation residuals and trends. The thermal contributors from greatest to least are: Horizontal feed arm, vertical feed arm, alidade, and finally the BUS. The gravity coefficients in this case are residual with respect to the "default" GBT pointing model. The differences are quite large. This was in part due to an error that was discovered in previous pointing model generation forced by the reconciliation of this analysis with previous models. Even after correcting the error, residual thermal distortions of the structure are evident and corrected by the methods of this memo.

The corresponding test of the model against the 11/20/03 data is shown in Figure 7 and Figure 8. Gravitation effects have essentially been removed since the residuals are with respect to the decouple Az/El models (AW and AN allowed to vary indepedently between the azimuth and elevation models). The thermal model compensates for about one-half of the total thermal trend (Figure 7, top subgraph). The residual error, after correction, for the entire eight hour period has a standard deviation of 3.2" and a mean error of 3.7". It's important to note that the mean error would be removed by a point-up and local pointing correction at the start of a scan. Currently unpublished results from Jim Condon indicate that the differential pointing accuracy of the GBT in these conditions is less than 1.5".

The trend line (Figure 7, "Meas-Pred") of the corrected elevation has a slope of –0.7" per hour and a residual from trend of 2.8". As it was with focus, the GBT is meeting at least Q band pointing requirements using these methods. A close look at these graphs also suggests that there may be a strong correlation between small changes in azimuth and the remaining elevation pointing residuals: It may be that we are seeing azimuth track unevenness.

5.2 Azimuth results

The azimuth model training results are shown in Figure 9. Once again, there are significant reductions in pointing residuals and trends, but it is worth noting that the model doesn't seem to perform as well during midday. The testing results in Figure 10 and Figure 11 indicate that the minor mis-match in gravity models may be responsible for a 4" offset. Beyond that the dataset doesn't seem to exercise the thermal correction model much, and the standard deviation of the corrected residual is 2.4". The trend line for the residuals exhibits a –0.15" per hour trend. Once again, the results indicate Q band performance at least.

6 Graceful degradations

It's likely that the availability of the temperature monitoring system will not be 100%: I.e., there will be occasional failures of temperature sensors. Currently we have had two failures in about three months of operation of 19 sensors total, both attributed to thermistor failure.

In the case that a sensor fails in a detectable way like failure to send data at the one-second intervals, the implementation of temperature corrections to pointing and focus should signal interested parties (operator, observer, etc.) that such a failure has occurred, and then continue to send corrections as best it can. Examples: If a sensor that fails is one of a symmetric pair like the elevation bearing sensors, then replace the average with the value of the remaining sensor. For anti-symmetric features, replace the difference with zero. It's likely that such strategies will produce slightly degraded performance but will still improve overall pointing and focus. Such strategies could be enumerated and tested when we progress from our prototype correction system to a production system.

7 Acknowledgements

These results would not have been possible without Richard Prestage's and Dana Balser's experimental results, Jim Condon's insights, and the PTCS instrumentation team: Jason Ray, J.D. Nelson, Randy McCollough, Paul Marganian, and Jeff Cromer.

Table 1. Temperature Sensor Locations, Names, Symbols.

Sensor Name[12]	Location	Structure Node	Symbol
gbtts1_2001	Feedarm tip	41020	T_{F1}
gbtts1_2005	Subreflector		T_{SR}
gbtts2_2001	BUS vertex right	144015R (Hoop 15, Rib +440)	T_{B1}
gbtts2_2002	Vertical feedarm right front	40140R	T_{F2}
gbtts2_2004	Vertical feedarm right rear	40180R	T_{F3}
gbtts3_2001	Vertical feedarm left front	40140L	T_{F4}
gbtts3_2002	BUS vertex left	144015L (Hoop 15, Rib -440)	T_{B2}
gbtts3_2003	Vertical feedarm left rear	40180L	T_{F5}
gbtts3_2004	Horizontal feedarm left	21430L	T_{H1}
gbtts4_2001	Horizontal feedarm right	21430R	T_{H2}
gbtts4_2002	Elevation bearing right	736	T_{E1}
gbtts4_2003	Elevation bearing left	731	T_{E2}
gbtts4_2004	BUS center left	120025L (Hoop 25, Rib –200)	T_{B3}
gbtts4_2005	BUS center right	120025R (Hoop 25, Rib +200)	T_{B4}
gbtts4_2006	BUS center	100025 (Hoop 25, Rib +000)	T_{B5}
gbtts5_2001	Alidade right front	217	T_{A1}
gbtts5_2002	Alidade left front	210	T_{A2}
gbtts5_2003	Alidade right rear	267	T_{A3}
gbtts5_2004	Alidade left rear	260	T_{A4}
Air	Weather2 air temp		T_{W2}

[12] Structural temperature sensors are labeled by the symbolic network name of the communications concentrator and the port number to which the sensor is connected.

Figure 1.Temperature Sensor Locations

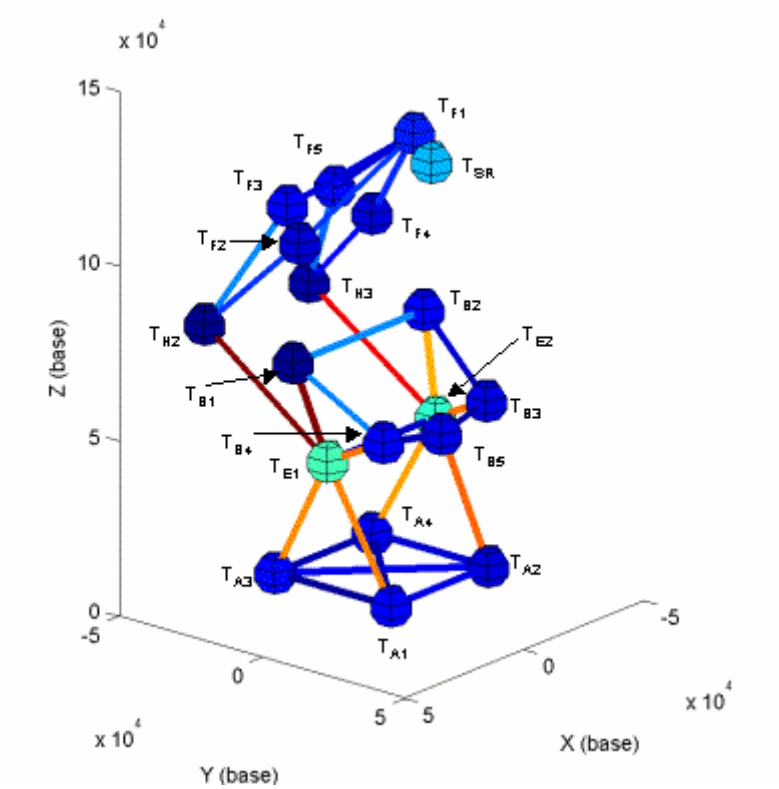

Table 2. Focus correction coefficients.

Term	**Coefficient** (mm/C or mm)	**Min-Max of associated T term**	**Significance**	**Parameter**
M_1	1.086	13.1	14.3	SR-Pri
M_2	-0.697	6.2	-4.3	VFA-Pri
M_3	3.981	15.6	62.0	HFA
M_4	-7.326	0.9	-6.8	BUS V1
M_5	-0.688	12.1	-8.3	BUS V2
M_6	-2.576	12.1	-31.2	BUS F
M_7	-180.630	0.0	0.0	Focus tracking offset
M_8	66.189	.7	43.1	Focus tracking sin term
M_9	196.949	0.6	110.8	Focus tracking cos term

Figure 2. Linear focus corrections versus scan.

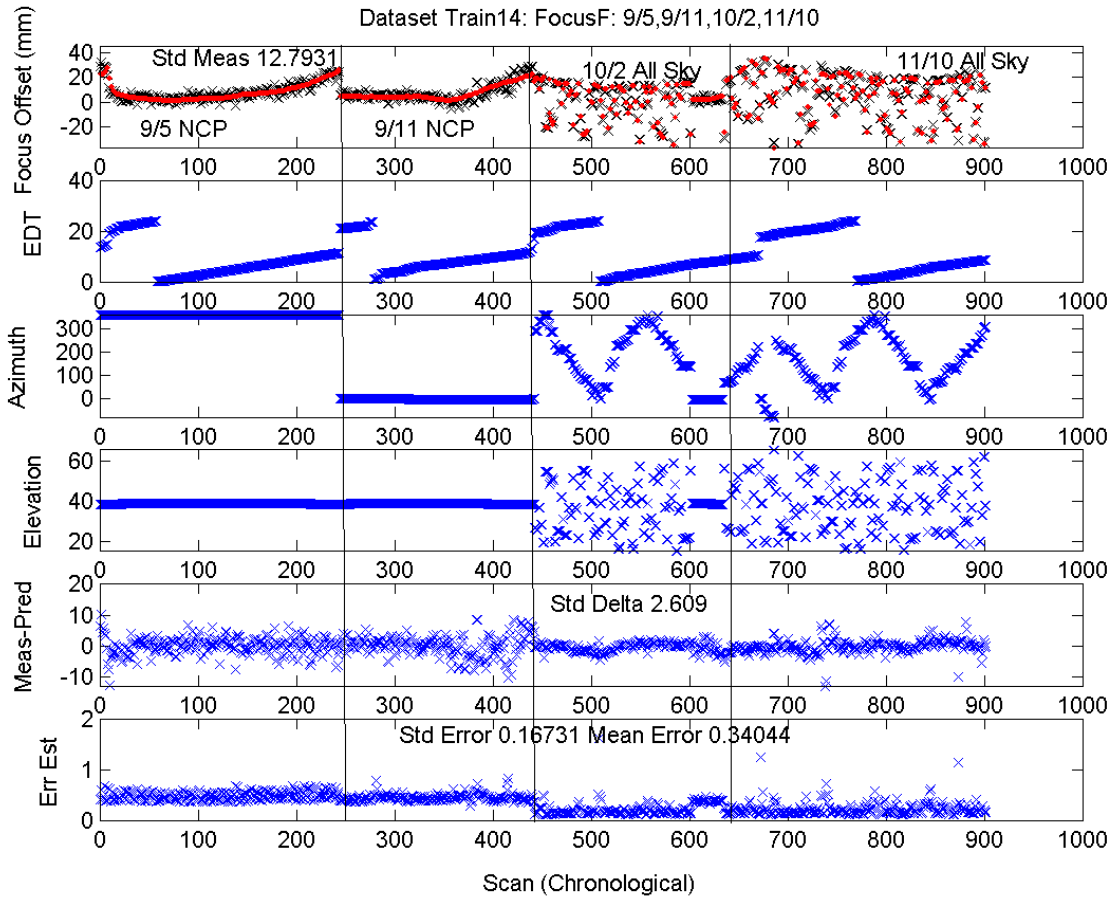

Figure 3. Linear focus corrections versus time of day (EDT).

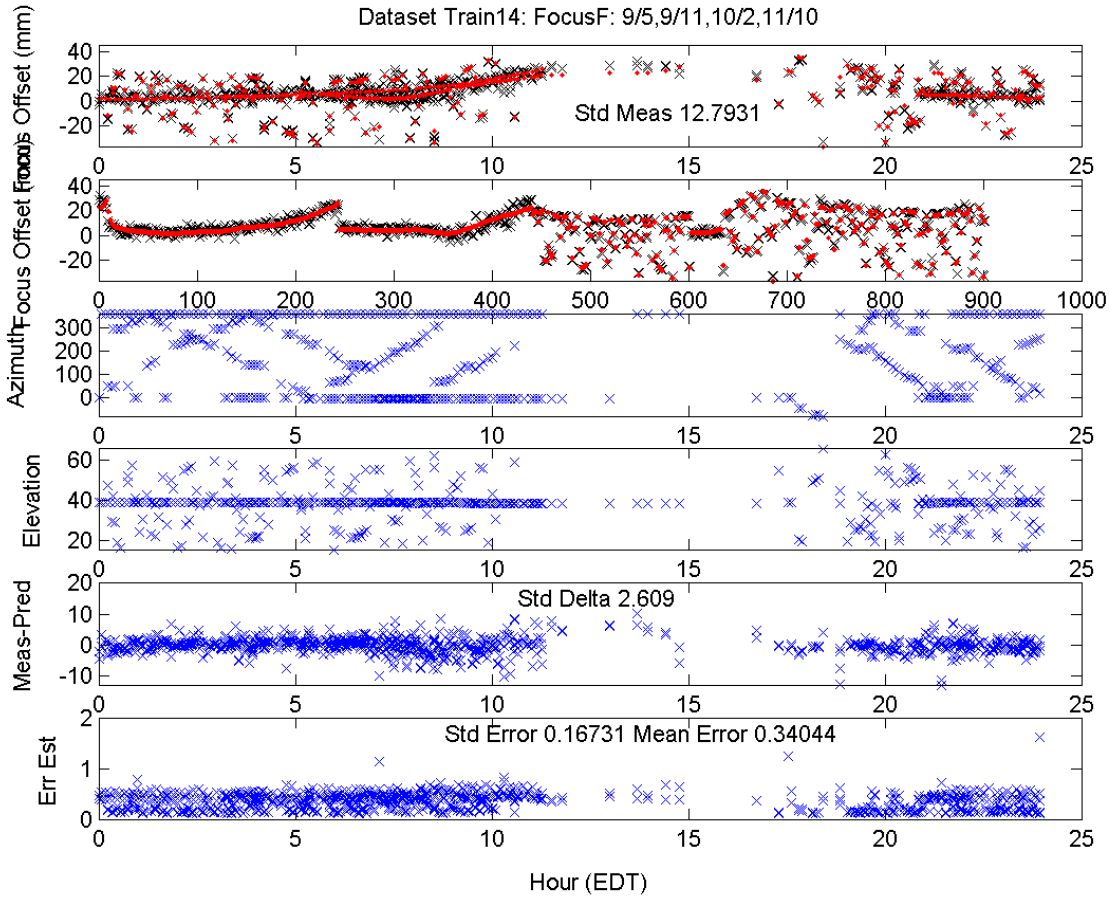

Figure 4. Focus model testing (chronological scan)

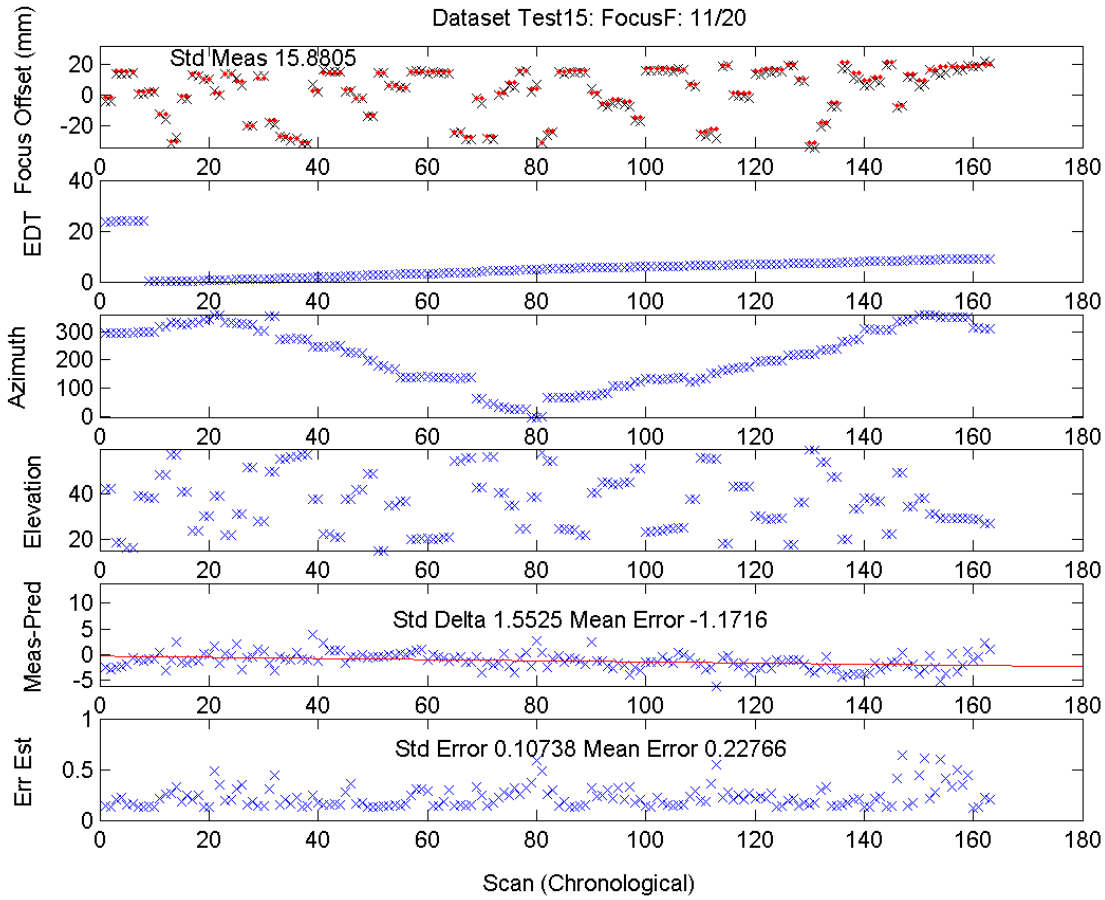

Figure 5. Focus model testing (EDT)

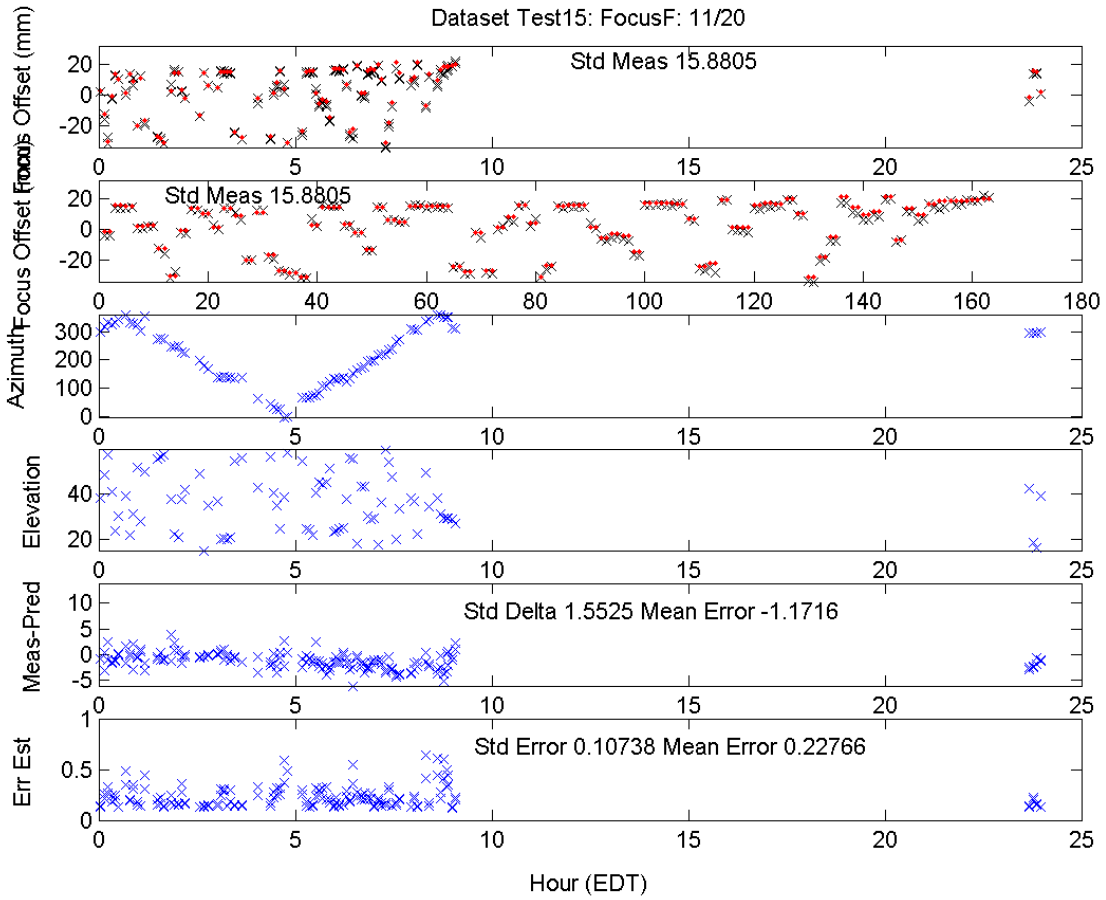

Table 3. Elevation correction coefficients.

Term	Coefficient (", "/C)	Min-Max of associated T term	Significance	Parameter
M_1	-4.6455	1.2	-5.3	BUS
M_2	1.7830	15.6	-27.8	HFA
M_3	4.4488	5.9	26.4	VFA
M_4	-8.4477	1.6	-14.0	Alidade
M_5	62.2218	0.0	+0.000	-IE,d(0,0)
M_6	-55.8624	0.7	-62.792	HZCZ,b(0,1)
M_7	-22.8268	0.9	-38.216	HZSZ,d(0,1)
M_8	2.4960	2.0	+2.169	-AW,c(1,0)
M_9	-1.3360	2.0	-1.750	AN,d(1,0)

Figure 6. Elevation model training (EDT)

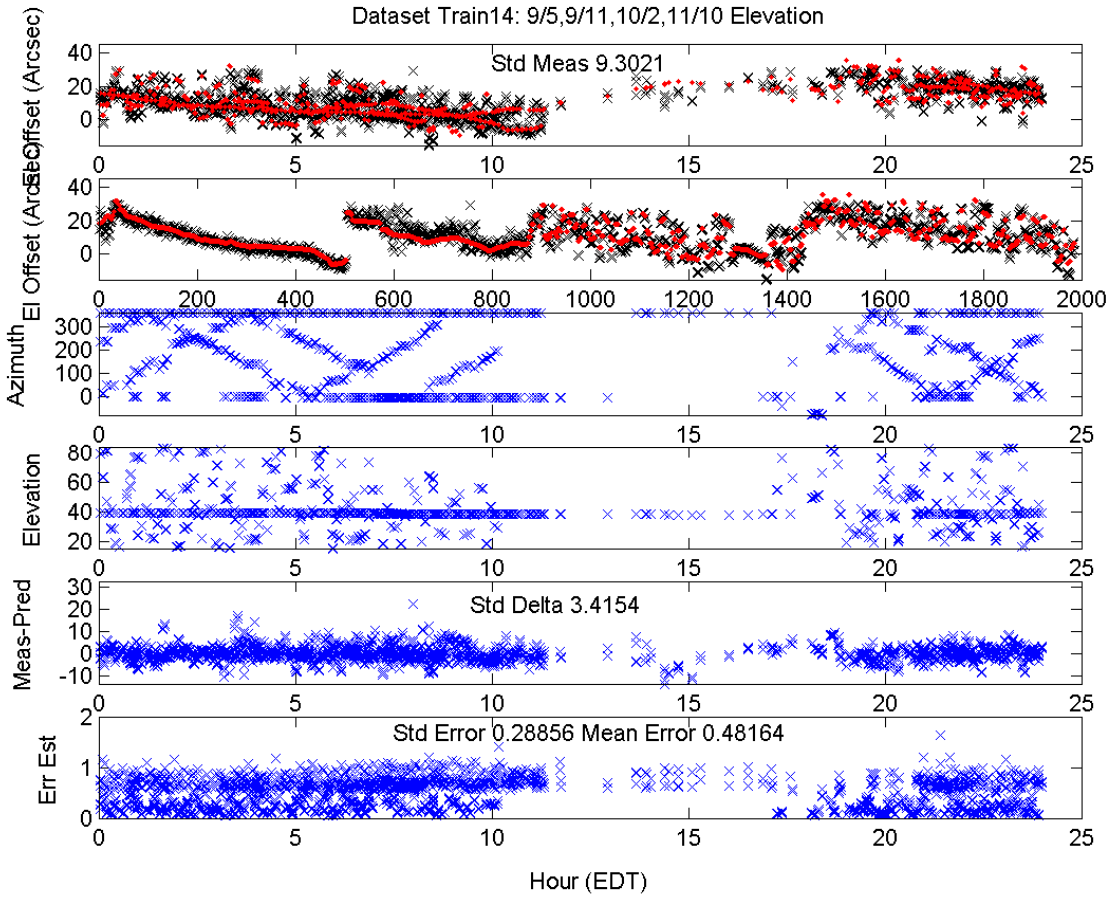

Figure 7. Elevation model testing (chronological scan)

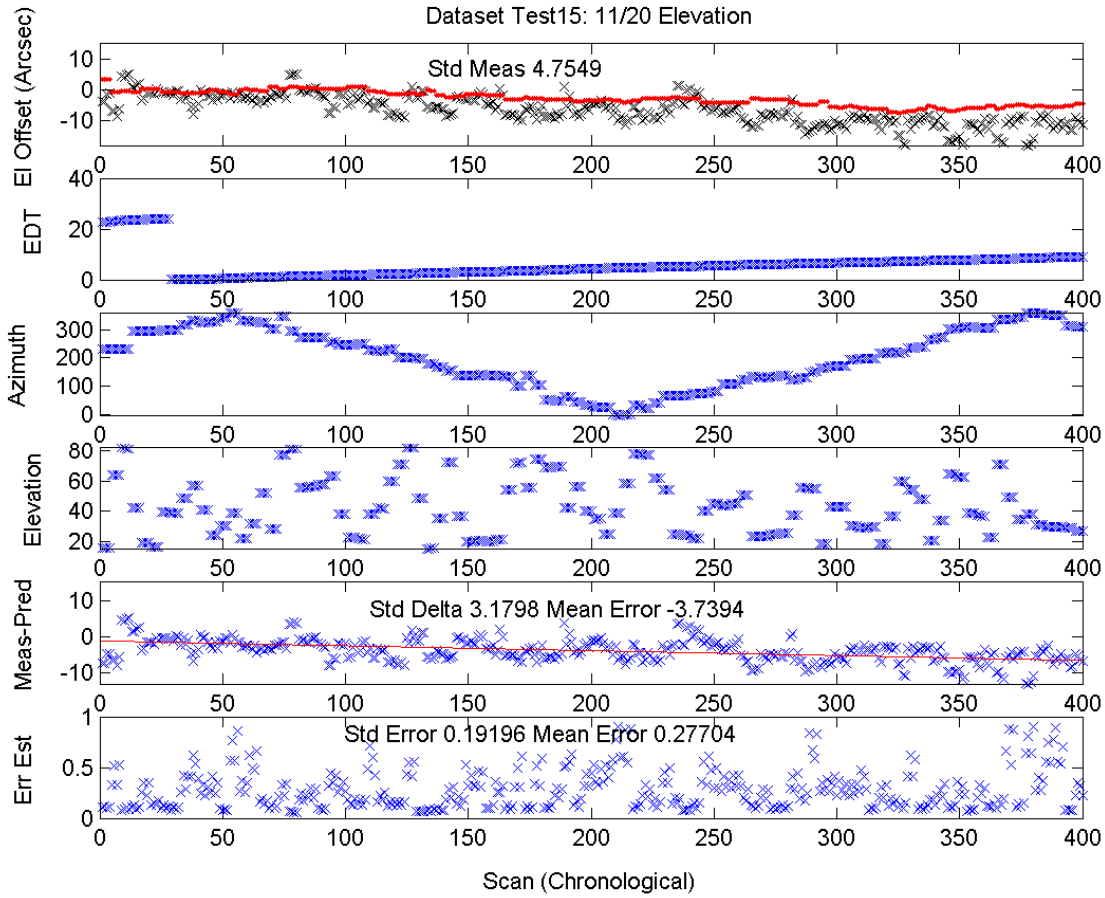

Figure 8. Elevation model testing (EDT)

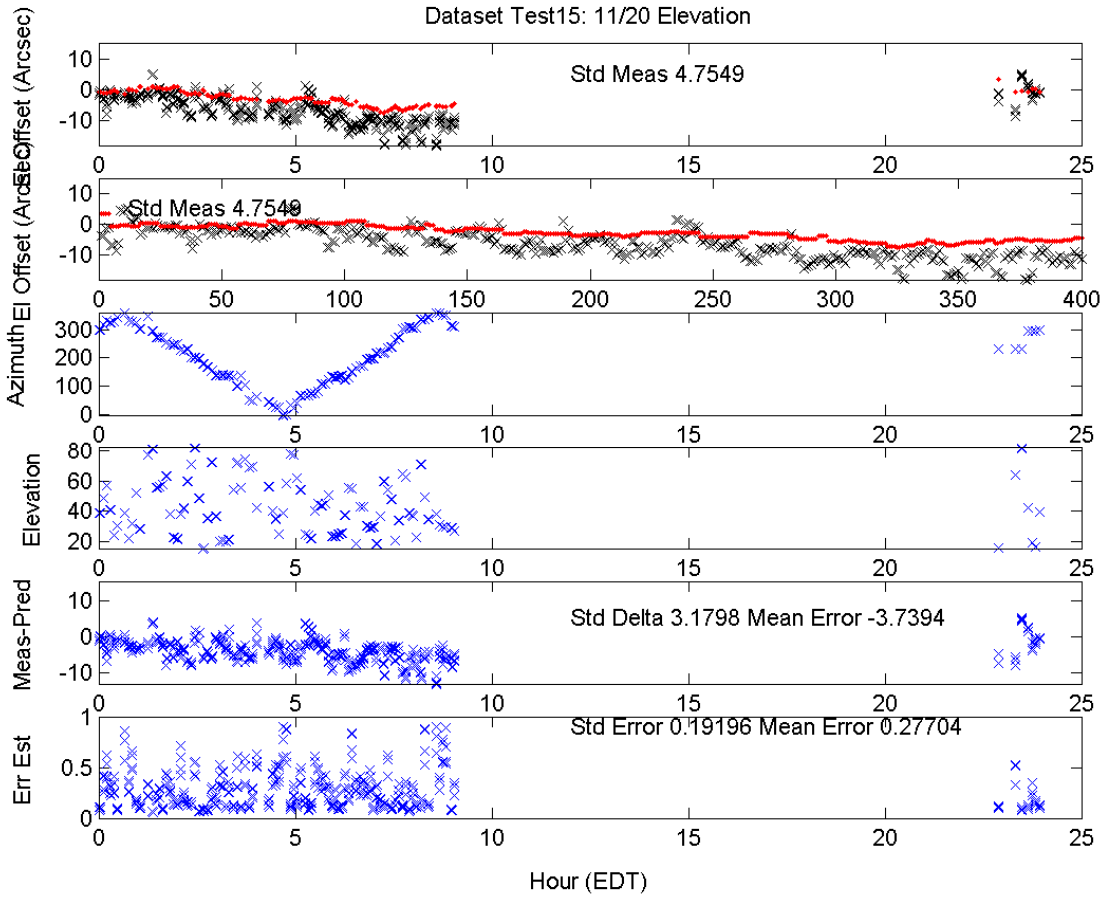

Table 4. Azimuth correction coefficients

Term	Coefficient (", "/C)	Min-Max of associated T term	Significance	Parameter
M_1	5.5862	4.0	22.4	Alidade
M_2	-8.0331	2.7	21.3	HFA
M_3	-1.6289	2.4	3.8	BUS
M_4	1.3683	2.0	2.8	VFA
M_5	3.4124	0.0	0.0	CA, d(0,0)
M_6	1.3223	0.7	1.0	NPAE, b(0,1)
M_7	3.5152	0.9	3.0	IA, d(0,1)
M_8	-2.4960	1.9	4.8	AW, b(1,1)
M_9	-1.3360	1.8	2.5	AN, a(1,1)

Figure 9. Azimuth model training (EDT)

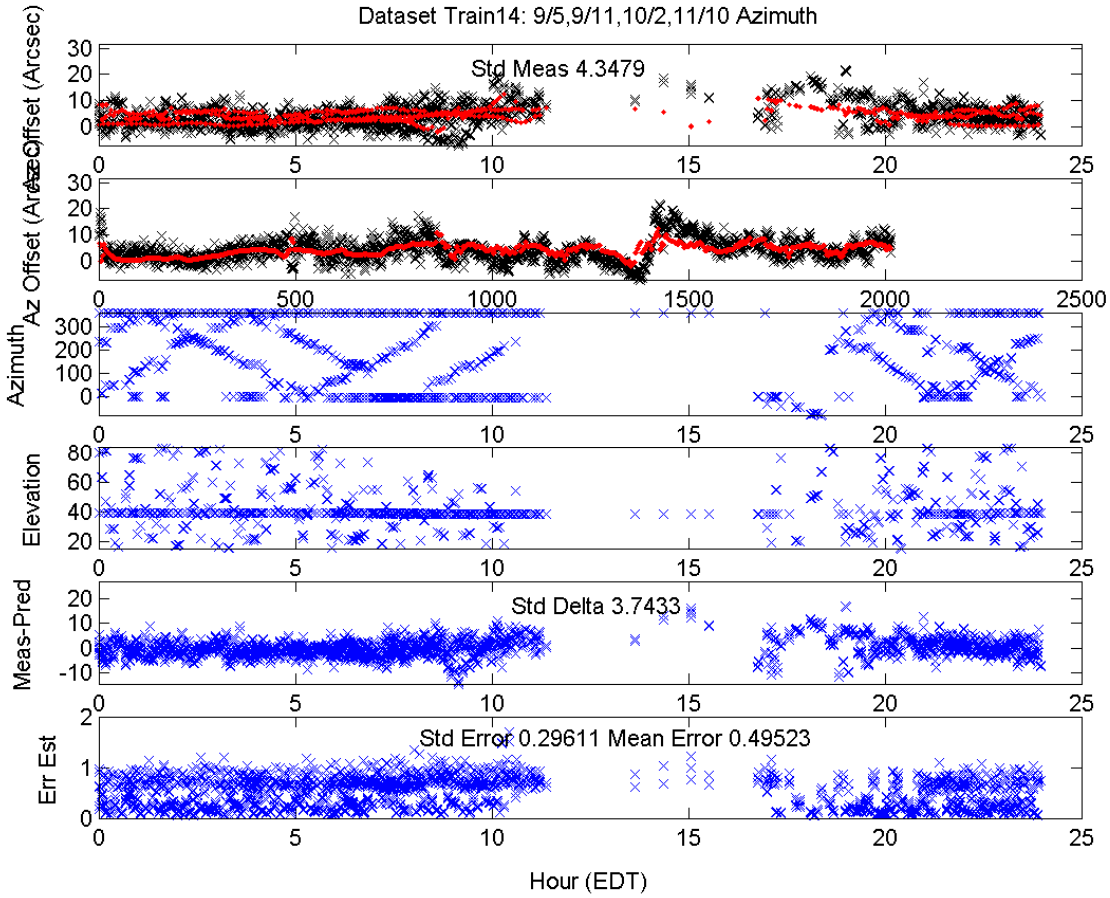

Figure 10. Azimuth model testing (chronological scan)

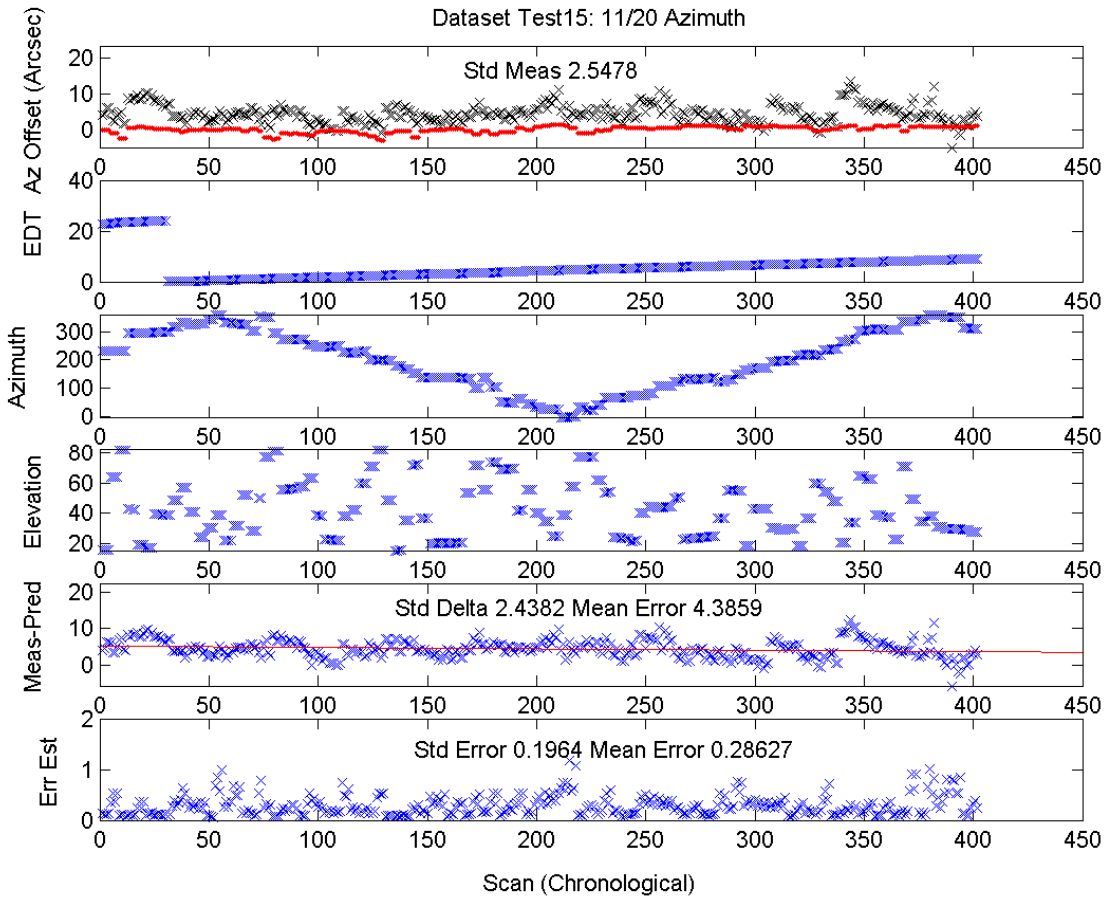

Figure 11. Azimuth model testing (EDT)